Metal-Enhanced Surface Plasmon-Coupled Phosphorescence

Michael J. R. Previte,[†] Kadir Aslan,[†] Yongxia Zhang,[†] and Chris D. Geddes*[,†,‡]

Institute of Fluorescence, Laboratory for Advanced Medical Plasmonics, Medical Biotechnology Center, University of Maryland Biotechnology Institute and Center for Fluorescence Spectroscopy, Medical Biotechnology Center, University of Maryland School of Medicine, University of Maryland, 725 West Lombard Street, Baltimore, Maryland 21201

Received: November 11, 2006; In Final Form: February 17, 2007

In this paper, we report the first observation of metal-enhanced surface plasmon-coupled phosphorescence (ME-SPCP) from 2,3,7,8,12,17,18-octaethyl-21H,23H-porphyrin platinum II (PtOEP) immobilized in 1% poly(vinyl chloride) (PVC) films on 47 nm continuous gold films coated with 20 and 80 nm silver colloids. In addition to the free space intensity enhancements, increased photostability decay rates, and additional short lifetime components for glass and gold substrates treated with silver colloids, we also observe a pronounced intensity enhancement and photostability of the SPCP signal from the PtOEP/PVC sample on the 47 nm Au films coated with 80 nm Ag colloids. In contrast, we observe a minor enhancement of the SPCP signal from the Au films coated with only 20 nm Ag colloids. The SPCP enhancement from the PtOEP complexes in 1% PVC films on Au films coated with Ag colloids is the first observation of ME-SPCP. In addition, we note the observation of two populations of near-field-induced plasmons: those facilitating ME-SPCP and noncoupled metal-enhanced free space phosphorescence.

1. Introduction

With an increasing demand for improved sensitivity and detectability of chromophores on surfaces and the respective application to biomedical assays, the study of fluorescent species close to metal surfaces has generated a great deal of recent interest.[1−6] The theory for fluorescent molecules in the presence of metal colloids has been extensively developed and experimentally demonstrated.[7−11] It has been experimentally realized and theoretically calculated that the extent of fluorescence enhancement on roughened metal surfaces, such as those created with metal colloids, is dependent on the degree of separation of the fluorophores from the respective protruding features of the modified substrates.[11−13] Consequently, maximum enhancement is attained when the distance of the chromophore from the nanosized metal features is optimized, such that the coupling of the dipole to the metal (mirror dipole effect) allows for the radiative process to occur before the excited-state energy of the dipole is dissipated through the molecule's nonradiative pathways (e.g., quenching of fluorophores in close proximity to a metal surface).[11−13]

Early experimental and theoretical work on the nature of chromophore metal interactions demonstrated that fluorescent lifetimes are dramatically affected by the interactions of excited-state molecules with metal surfaces.[7−11,14−16] Because of the the metal-chromophore interactions, it was predicted theoretically and shown experimentally that the fluorophores exhibited increased brightness, increased absorption cross-sections, and decreased lifetimes, which suggested that radiative decay rates were increased and ultimately, increased photostability.[7−11,14−21] Earlier studies suggested that the modified radiative decay rates of fluorophores were dependent in a nontrivial way on the size and shape of metallic surfaces or particles and the distance and orientation of the molecule, relative to the particle.[11,22,23] More recent studies suggest an alternative model, the radiating plasmon model (RPM), whereby nonradiative energy transfer occurs from excited distal fluorophores to the surface plasmons, which subsequently radiate the photophysical characteristics of the coupling fluorophores.[6,24,25] Within the framework of the recently developed radiating plasmon model, our groups have worked extensively in the area of metal-enhanced fluorescence (MEF) to provide a great deal of experimental support for this model of metal-chromophore interactions.[6,24−31] Metal-enhanced phenomena have not been limited to studies of fluorescence coupling to surface plasmons. For example, enhanced phosphorescence emission and increased decay rates were recently reported for 2,3,7,8,12,17,18-octaethyl-21H,23H-porphyrin platinum II (PtOEP) complexes in polymer films near nanotextured silver surfaces.[32] In addition, metal-enhanced phosphorescence for Rose Bengal on silver island films was also reported in the most recent report of metal-enhanced phosphorescence (MEP).[33] In each of these reports, intensity enhancements and decreased lifetimes were observed for these compounds in close proximity to the metal surfaces.

In addition to the changes in the photophysical properties of chromophores in close proximity to metal nanoparticles, fluorescence near-field emission is also known to couple to surface plasmons at continuous metal surfaces.[9,34−36] The radiating plasmon model (RPM) also suggests that Förster energy distances and overall donor/acceptor system quantum yields increase in the presence of metal nanoparticles.[24] Consequently, it has been further proposed that this model may explain the observation of surface plasmon-coupled emission (SPCE) (alternatively, surface plasmon-coupled fluorescence spectroscopy[2]) in lieu of fluorescence quenching[37] for fluorophores in close proximity to continuous metal surfaces.[38,39] Because the propagating electromagnetic fields for surface plasmons at

* Corresponding author. E-mail address: geddes@umbi.umd.edu.
† Institute of Fluorescence.
‡ Center for Fluorescence Spectroscopy.

10.1021/jp0674773 CCC: $37.00
Published on Web 03/30/2007

interfaces propagate with a preferred direction and polarization, it was soon realized that the inherent isotropic fluorescence emission from a population of randomly oriented fluorophores close to metal surfaces would lend to directional and polarized emission.[9,34,35,40] As a result, it became possible to achieve better detectability of fluorophores at the metal interfaces and facilitate the detection of surface bound biomolecules.[2] Recently, we also observed that slower decaying chromophores, such as phosphorescent and chemiluminescent species, can couple to surface plasmons.[41] As a result, in addition to SPCE the phenomena of surface plasmon-coupled chemiluminescence (SPCC) and surface plasmon-coupled phosphorescence (SPCP) now expand the applicability of surface plasmon-coupling phenomena to the measurement of biomolecular interactions on/at surfaces for more weakly emitting chromophores, most notably phosphorescence, which are useful in the studies of protein dynamics and alkaline phosphatase studies.[1,42−44]

In this paper, we report the first observation of metal-enhanced surface plasmon-coupled phosphorescence (ME-SPCP) from PtOEP immobilized in poly(vinyl chloride) (PVC) films on 47 nm thick continuous gold films coated with Ag colloids. We show that it is possible to combine the advantages of metal-enhanced emission, such as increased photostabilities, intensity enhancements and increased system radiative rates with the directional emission benefit of surface plasmon-coupled emission. In accord with the inherent properties of metal-enhanced emission, our results verify the presence of MEP from PtOEP/PVC samples on glass substrates coated with 20 and 80 nm colloids, while we also confirm the first observation of ME-SPCP by comparing the intensity, lifetime, and photostability decay rates for ME-SPCP with the free space isotropic MEP from the PtOEP/PVC samples on 20 and 80 nm colloid-coated continuous gold films 47 nm gold thick. In addition, we believe that this is the first observation of two populations of fluorophore-induced plasmons within the same system: ME-SPCP and noncoupled metal-enhanced free space phosphorescence (MEP).

2. Theory

2.1. MEF. According to the radiating plasmon model, nonradiative energy transfer occurs from the excited fluorophores distal to the surface plasmon electrons in noncontinuous films.[24,25] The surface plasmons, in turn, radiate the photophysical characteristics of the coupling fluorophores. In essence, the system radiates as a whole.[24,25] As a result, the system exhibits modified overall radiative rates. Ultimately, the increased radiative rate for the system lends to enhanced fluorescence signals or increased quantum yields for fluorophores in close proximity to metallic structures, which are represented by the following equation:

$$Q_m = (\Gamma + \Gamma_m)/(\Gamma + \Gamma_m + k_{nr}) \quad (1)$$

where Γ is the unmodified system radiative decay rate, Γ_m is the metal-modified radiative decay rate, and k_{nr} are the nonradiative decay rates.[4,6,30] The metal-modified lifetime, τ_m, of a fluorophore is decreased by the increased system radiative decay rate according to the equation

$$\tau_m = 1/(\Gamma + \Gamma_m + k_{nr}) \quad (2)$$

When the particles are spherical and have sizes comparable to the incident wavelength of light (i.e., in the Mie limit) the extinction properties of the metal particles, which are expressed as a combination of absorption (C_A) and scattering cross-sections (C_S), determine the intensity of fluorophore-coupled plasmon radiation

$$C_E = C_A + C_S = k_1 \,\mathrm{Im}(\alpha) + \frac{k_1^4}{6\pi}|\alpha|^2 \quad (3)$$

where $k_1 = 2\pi n_1/\lambda_o$ is the wavevector of the incident light in the surrounding medium (typically, air, water, or polymer film), α is the polarizability of the sphere with radius r, n_1 is the refractive index of the medium, and λ_o is the incident wavelength. The term $|\alpha|^2$ is the square of the modulus of α

$$\alpha = 4\pi r^3(\epsilon_m - \epsilon_1)/(\epsilon_m + 2\epsilon_1) \quad (4)$$

where ϵ_1 and ϵ_m are the dielectric and the complex dielectric constants of the metal, respectively.[24]

2.2. SPCE. The theory of SPCE has its origins in the theory of surface plasmon resonance, which is covered in detail elsewhere.[2,9,24,40,45] Briefly, the coupling of light emission from a chromophore to metal surfaces depends on the matching of the wavevector of the incident light (k) with the wavevector of the surface plasmons (k_{sp}). The wavevector of the incident light is given by

$$k_p = \frac{2\pi}{\lambda} = \frac{n_p\omega}{c} = n_p k_o \quad (5)$$

where n_p is the refractive index of the prism, λ is the wavelength, ω is the frequency in radians/s, and k_o is the wavevector in free space. The wavevector (k_{sp}) for the surface plasmon is given by

$$k_{sp} = k_o\left(\frac{\epsilon_m\epsilon_s}{\epsilon_m + \epsilon_s}\right)^{1/2} \quad (6)$$

where ϵ_m and ϵ_s are the real parts of the dielectric constants of the metal ($\epsilon_m = \epsilon_r + i\epsilon_i$) and the sample ($\epsilon_s = \epsilon_r + i\epsilon_i$) above the metal film (Figure 1 left). The surface plasmon phenomenon persists when the x-axis component wavevector of the emissive light from the chromophore (incident light) equals the wavevector of the surface plasmon.[39] If the wavevector of the incident light on the prism is given by $k_p = k_o n_p$, the x component or projection of the wavevector along the interface is $k_x = k_o n_p \sin\theta_i$, where θ_i is the incidence angle in the prism measured from the normal to the metal surface. It follows that the conditions for SPR excitation are met when

$$k_{sp} = k_x = k_o n_p \sin\theta_{sp} \quad (7)$$

where θ_{sp} is the surface plasmon-coupling angle. From this equation, it follows that the reflectivity and transmissivity of incident light at the metal/dielectric interface are determined by θ_{sp}.

The reflectivity at the surface below the θ_{sp} is very high due to the presence of an evaporated metal layer that acts as a mirror and reflects most of the transmitted light.[2] At just above θ_{sp}, the metal surface acts as a resonator for incident light propagating from the emitting dye molecule, and gives rise to the resonant excitation of surface plasmons, which reradiate according to the dispersion curve for surface plasmons. The surface plasmon dispersion curves are predicted with Fresnel calculations, which take into account the interactions of light impinging upon media with multiple phases.[46]

3. Methods and Materials

The reverse Kretschmann (RK) configuration is implemented for all free space and SPCP measurements such that the sample

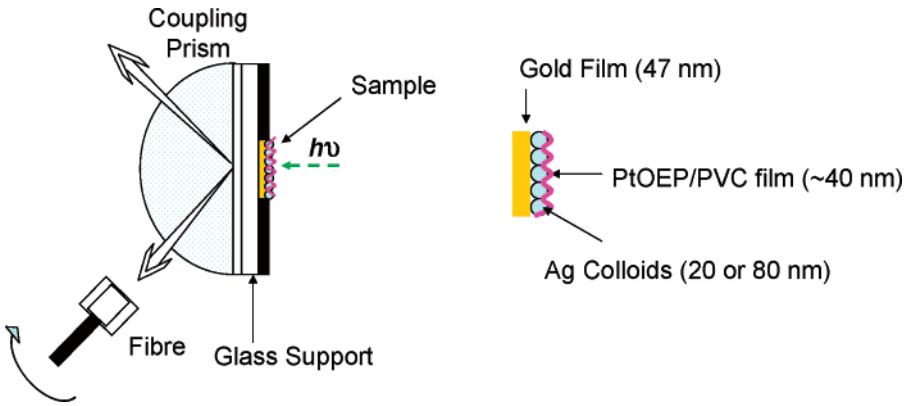

Figure 1. ME-SPCP experimental detection scheme (left) and sample geometry (right).

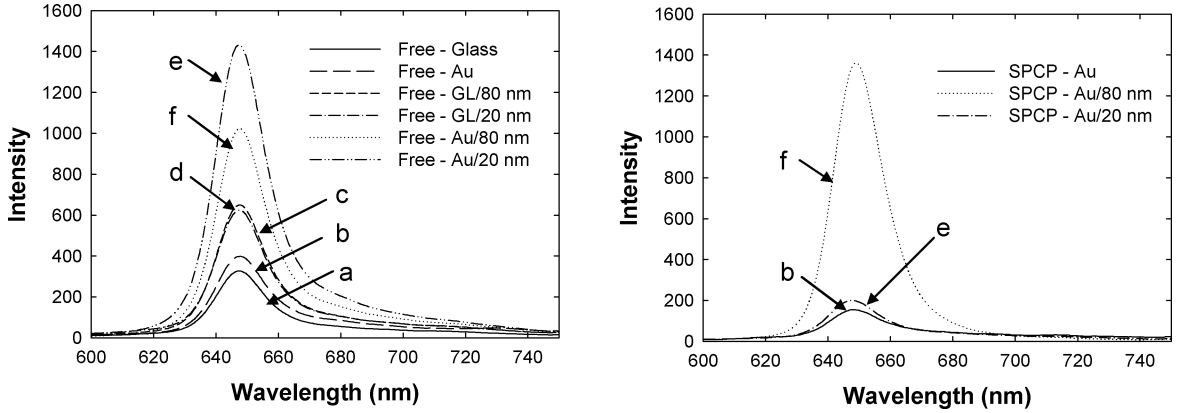

Figure 2. Free space (left) and SPCP (right) emission spectra of 0.50 mM PtOEP in 1% PVC films spin-coated at 4000 rpm for 3 min on: (a) glass slides; (b) continuous gold films 47 nm thick; glass slides with (c) 20 nm Ag colloids (d) 80 nm Ag colloids; and continuous gold films (Au) 47 nm thick incubated with (e) 20 nm Ag colloids and (f) 80 nm Ag colloids.

is excited from the air or sample side and the angle of incidence was normal to the sample surface (Figure 1, left).[15] The SPCP (prism side or back plane) for the PtOEP/PVC mixtures was collected at the critical angle for this setup, which was approximately 72°. Free space phosphorescence emission was measured at 175 and 190° (excitation side or front plane). For detection, a 600 μm fiber was mounted on a rotation stage, which could be rotated 360 degrees around the sample. Angular measurements were determined from the labeled gradations scribed on the rotation stage at 1° intervals. Au films were deposited on silanated glass slides by vapor deposition using an EMF Corp. (Ithaca, NY) vapor deposition instrument. Film thicknesses were monitored during the deposition process with an Edwards FTM6 film thickness monitor. Silver colloid solutions, 20 and 80 nm, were purchased from Ted Pella, Inc (Redding, CA). Colloidal gold and glass substrates were prepared by incubating glass and Au slides overnight at 4° in 3 mL of the respective 20 and 80 nm colloid solutions, which had working concentrations of 7.0×10^{11} and 1.1×10^{10} particles/mL, respectively. Samples of PtOEP complexes were dissolved in toluene and mixed with 10% PVC stock solutions. Final PVC solutions were mixed at 1% PVC in toluene with a final concentration of 0.48 mM PtOEP. Forty microliters of the PVC mixtures were then spin-coated on the substrates. Previously published data by Gryczynski et al.[47] that describes the relationship between polymer percent composition and film thickness was fit to a cubic polynomial function, which was subsequently used to estimate PVC film thicknesses for these experiments (data not shown).[41] The PVC films for the samples in this experiment were estimated to be 40 nm thick.[47] A schematic depicting the sample geometry is shown in Figure 1, right. Extinction coefficient plots for 20 and 80 nm silver particles (Figure 3) were simulated using MieCalc 1.5 (Simuloptics GMbH, Schwabach, Germany).

All phosphorescence emission measurements were made with an Ocean Optics HD2000 spectrofluorometer. Photostability curves for all samples are collected at a time interval of 1 s over a 400 s total collection time. Photostability decay results shown in Table 2 were fit to a double exponential decay model, $I(t) = A_1e^{-k_1t} + A_2e^{-k_2t}$, using Matlab's nonlinear least-squares optimization routine where k_i is the decay rate of component i and A_i is its amplitude such that $\sum_i A_i = 1.0$. The contribution of each component to the steady-state decay time is given by

$$f_i = \frac{A_i k_i}{\sum_i A_i k_i} \tag{8}$$

the mean decay time is given by

$$\bar{k} = \sum_i f_i k_i \tag{9}$$

and the amplitude-weighted decay time photostability is given by

$$\langle k \rangle = \sum_i A_i k_i \tag{10}$$

Lifetime measurements for free space emission and SPCP from PtOEP samples were measured using a submicrosecond Xenon flashlamp operating at a frequency of 300 Hz (IBH,

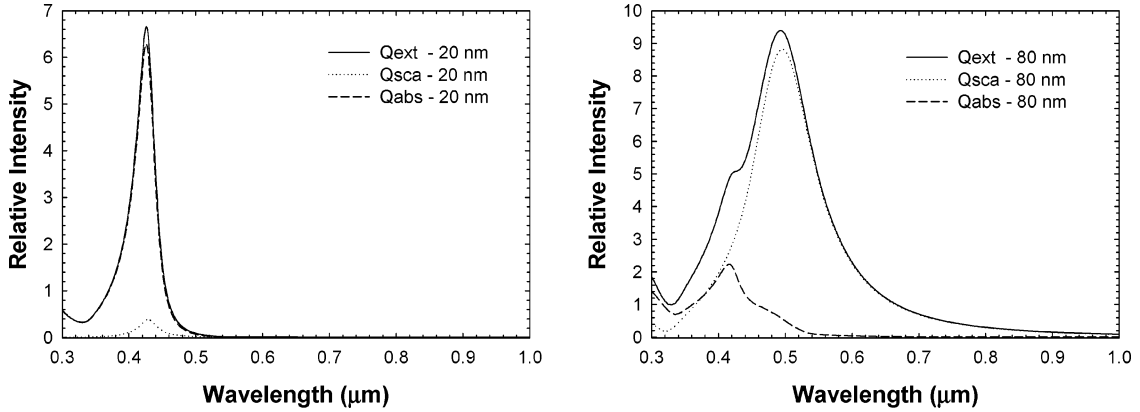

Figure 3. Theoretical plots of extinction, scattering, and absorption cross-sections for 20 nm (left) and 80 nm (right) Ag colloids. Extinction coefficients calculated using MieCalc 1.5 (Simuloptics GMbH, Schwabach, Germany).

TABLE 1: Recovered Lifetimes for PtOEP in 1% PVC on MEP−SPCP Substrates

sample configuration:	A_1	τ_1 (μs)	A_2	τ_2 (μs)	$\bar{\tau}$	$\langle t \rangle$	χ^2
glass-free (1 exp)	936.0	47.2					.959
Au-free thin (1 exp)	1958	51.5					1.00
20 nm Ag on glass-free	168.4	56.6	708	6.58	16.2	40.2	.943
80 nm Ag on glass-free	180.5	62.0	440	4.82	21.5	52.9	.916
20 nm Ag on Au-free	1025	55.6	4900	7.78	16.1	36.4	1.01
80 nm Ag on Au-free	1595	55.5	2580	5.76	25.0	48.4	.996
Au-SPCP	1200	52.9					.934
20 nm Ag on Au-SPCP	152.1	44.5					.956
80 nm Ag on Au-SPCP	114.6	50.7					.958

Model 5000XeF) as the excitation source, a cooled high-speed PMT detector head for photon counting (PMC-100, Becker-Hickl), and a gated photon counter/multiscalar card (MSA-300, Becker-Hickl). To excite the PtOEP/PVC samples, a bandpass filter HQ535/50 was placed in the path of the Xenon flashlamp. Lifetime analysis fitting was performed using FluoFit software provided by Picoquant GmbH.

Lifetime data was fit using a multiexponential model

$$I(t) = \int_{-\infty}^{t} IRF\,(t') \sum_{i=1}^{n} \alpha_i e^{-t-t'/t_i}\,dt' \tag{11}$$

where $IRF\,(t')$ is the measured instrument response, τ_i is the lifetime of component i and α_i is its amplitude where $\sum_i \alpha_i = 1.0$. The contribution of each component to the steady-state intensity is given by

$$f_i = \frac{\alpha_i \tau_i}{\sum_i \alpha_i \tau_i} \tag{12}$$

the mean decay time is given by

$$\bar{\tau} = \sum_i f_i \tau_i \tag{13}$$

and the amplitude-weighted lifetime is given by

$$\langle \tau \rangle = \sum_i \alpha_i \tau_i \tag{14}$$

Lifetime data are tabulated in Table 1.

4. Results

We compared the lifetimes of SPCP and free space emission for the Pt/porphyrin complexes in 1% PVC films (approximately 40 nm thick) on the different substrates (Table 1). We found that the free space phosphorescence lifetimes for PtOEP/PVC samples on glass substrates (47.2 μs) are slightly shorter than the lifetime on 47 nm gold films (51.5 μs). We measured a long and short lifetime component for glass substrates coated with 20 nm Ag colloids (56.6 and 6.58 μs) and glass substrates coated with 80 nm Ag colloids (62.0 and 4.82 μs). In addition, we determined that there exists a long and short lifetime component for the PtOEP/PVC samples on Au films coated with 20 nm Ag colloids (55.6 and 7.78 μs) and for Au films coated with 80 nm Ag colloids (55.5 and 5.76 μs). The SPCP lifetimes for the PtOEP/PVC samples on 47 nm Au films, 20 nm Ag colloid/gold substrates, and 80 nm Ag colloids/gold substrates are all single-exponential decays, 52.9, 45.5, and 50.7 μs, respectively.

From PtOEP/PVC samples on the glass substrates coated with 20 and 80 nm Ag colloids, we observed an enhancement of the free space phosphorescence emission (Figure 2, left). Although the calculated scattering extinction coefficient for 80 nm particles is greater (Figure 3, right) than that for the 20 nm particles (Figure 3, left),[48,49] we measured only slight differences in the intensity of the glass substrates incubated with 80 nm colloids versus those incubated with 20 nm colloids. On the gold substrates, the free space phosphorescence intensity is more enhanced than the free space emission from glass (Figure 2, left). For the gold substrates, we also observe that the free space phosphorescence from the 20 nm Ag colloid/gold substrate is greater than that from the 80 nm Ag colloid/gold substrates.

In addition to the free space intensity measurements for the colloids on the gold substrates, we also measured the directional SPCP intensity measurements (Figure 2, right). From these results, we observed a nine-fold enhancement of the SPCP signal from the PtOEP/PVC samples on the 80 nm Ag colloid/gold substrates versus SPCP signal from gold substrates without colloids. We also note a minor enhancement (1.3-fold) of the SPCP signal from the PtOEP/PVC samples on the 20 nm Ag colloid/gold substrates. The SPCP enhancement from the PtOEP/PVC samples gold films-coated Ag colloids is the first observation of ME-SPCP, and these results are consistent with the RPM and the size dependent enhancement from different sized colloids.[24,25]

Photostability decay results for the PtPOEP/PVC samples on the different substrates (Figure 4) were fit to two exponential decay models and tabulated in Table 2. We found that all decay rates have both fast and slow components (Table 2). We also calculated the mean decay time, $\bar{k}$, from eq 5 and the amplitude-weighted decay time, $\langle k \rangle$ from eq 6. From the amplitude-

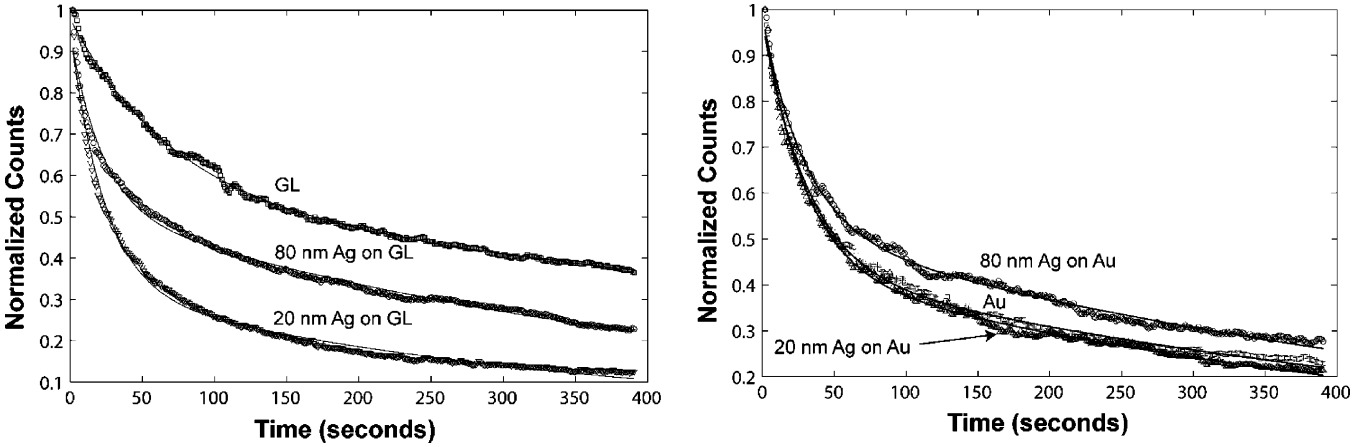

Figure 4. Photostability traces 0.50 mM PtOEP in 1% PVC films spin-coated at 4000 rpm for 3 min on glass slides (left) and continuous gold films 47 nm thick (right) incubated with 20 and 80 nm Ag colloids.

TABLE 2: Recovered Free and Plasmon-Coupled Phosphorescence Photostability Decay Rates for 0.50 mM PtOEP in 1% PVC Films Spin-Coated at 4000 rpm for 3 min on Glass Slides and Continuous Gold Films 47 nm Thick Incubated with 20 and 80 nm Ag Colloids[a]

sample configuration:	A_1	k_1 (s^{-1})	k_2 (s^{-1})	A_2	$\bar{k}$	$\langle k \rangle$
glass	0.56	1.42×10^{-2}	1.00×10^{-3}	0.44	1.31×10^{-2}	6.81×10^{-3}
Ag (20) on GL	0.36	4.22×10^{-2}	2.83×10^{-3}	0.66	4.09×10^{-2}	2.88×10^{-2}
Ag (80) on GL	0.56	4.54×10^{-2}	2.20×10^{-3}	0.44	4.29×10^{-2}	2.12×10^{-2}
Au film (47 nm)	0.45	3.19×10^{-2}	1.76×10^{-3}	0.55	3.06×10^{-2}	1.83×10^{-2}
Ag (20) on Au	0.44	3.43×10^{-2}	1.95×10^{-3}	0.56	3.29×10^{-2}	2.01×10^{-2}
Ag (80) on Au	0.53	3.39×10^{-2}	1.78×10^{-3}	0.47	3.21×10^{-2}	1.69×10^{-2}
SPCP-Au	0.51	1.20×10^{-2}	1.18×10^{-3}	0.49	1.89×10^{-2}	1.04×10^{-2}
SPCP-Au/20	0.31	4.73×10^{-2}	2.34×10^{-3}	0.69	4.63×10^{-2}	3.32×10^{-2}
SPCP-Au/80	0.47	9.18×10^{-3}	2.42×10^{-4}	0.53	8.98×10^{-3}	5.00×10^{-3}

weighted decay rate, we can delineate the relative contribution of each decay component to the overall decay rate.

From the normalized free space photostability curves for the PtOEP/PVC sample on glass substrates coated with 20 and 80 nm silver colloids, we observed that the PtOEP complex is least photostable on the glass substrates coated with 20 nm colloids and most photostable on the unmodified glass substrate (Figure 4, left). The normalized free space photostability curves for the PtOEP/PVC sample on 47 nm gold film substrates and 47 nm gold film substrates coated with 20 and 80 nm silver colloids showed that the PtOEP complex is least photostable on the gold films coated with 20 nm colloids and most photostable on the gold films coated with 80 nm colloids (Figure 4, right). In addition, to the free space photostability measurements, we also measured the SPCP photostability decay rates for the PtOEP complex on the gold substrates (plots not shown). We found that the PtOEP complex on the gold substrates coated with the 80 nm silver colloids had the greatest photostability, while the gold substrates coated with the 20 nm silver colloids was the least photostable, as expected.

5. Discussion

5.1. MEP. Drawing on the radiating plasmon model that was previously described[24,25] and outlined in the theory section above, we provide a pictorial representation of our interpretation of the phenomenon of ME-SPCP (Figure 5). At the maximum emission wavelength of the PtOEP complex, the scattering efficiency ($Q_S = C_S/\pi r^2$, where r is the radius of the metal particle), which typically accounts for emission enhancements, for 80 nm Ag particles is substantially larger than Q_S for the 20 nm Ag particles. In addition, the absorption efficiency ($Q_A = C_A/\pi r^2$), which typically accounts for quenching in the presence of metal surfaces, is negligible for both 20 and 80 nm particles (Figure 3). From eq 3, it is expected that larger metal colloids induce larger system metal-enhanced emission effects. Because larger emission intensity enhancements arise from the larger metal particles, which are indicative of increased quantum yields in the presence of larger particles (Q_m), it follows from eq 1 that the metal-modified radiative decay rates (Γ_m) increase with particle size, and that the metal-modified lifetimes will decrease (τ_m).

The radiative decay rates and quantum efficiency of a chromophore in the presence of a metal surface (i.e., metal colloids) depend on the proximity of the chromophore to the metal sphere.[50] Thus, the extent of energy transfer to a surface varies as a function of the chromophore's distance, r, of the chromophores to the metal surface and can be characterized by two potential descriptions of energy transfer processes, fluorescence resonance energy transfer (FRET) and surface energy transfer (SET).[51,52] The characteristic FRET relationship, which describes the energy transfer rate, k_{FRET}, of two interacting dipoles at very close distances (<10 Å), is written as

$$k_{FRET} = \left(\frac{1}{\tau_D}\right)\left(\frac{R_o}{r}\right)^6 \tag{15}$$

where τ_D is the lifetime of the donor and R_o is the Förster distance.[53] On the other hand, at intermediate distances (20−300 Å) surface energy transfer is the dominant process,[51,52] and the SET relationship is written as

$$k_{SET} = \left(\frac{1}{\tau_D}\right)\left(\frac{d_o}{d}\right)^4 \tag{16}$$

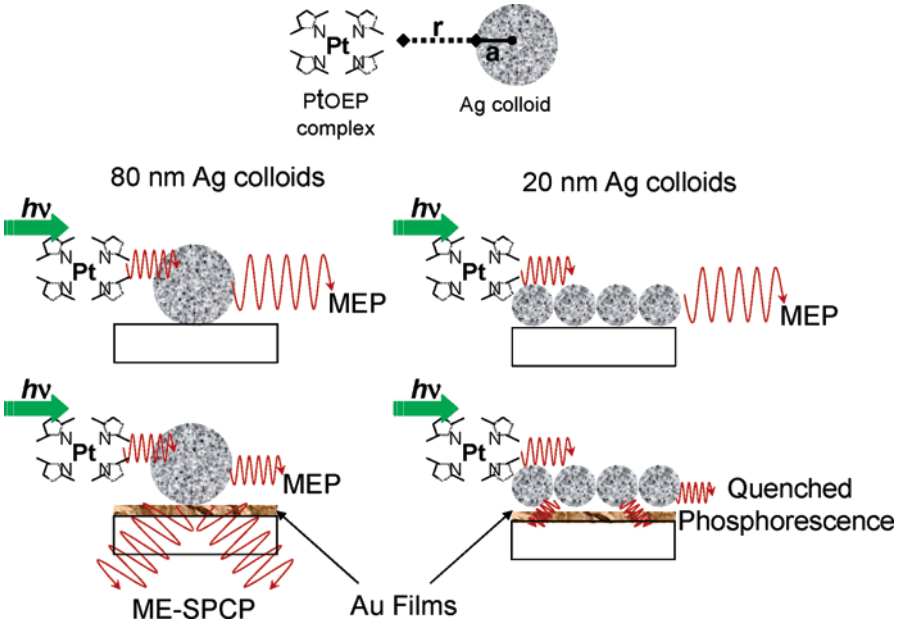

Figure 5. ME-SPCP illustration for both glass and continuous gold films 47 nm thick with 20 and 80 nm Ag colloids respectively.

where the characteristic distance length is given by

$$d_o = \left(0.525\frac{c^3\Phi_D}{\omega^2\omega_F k_F}\right)^{1/4} \quad (17)$$

and is a function of the donor quantum efficiency, Φ_D, the frequency of the donor electronic transition, ω, and the Fermi frequency, ω_F, and Fermi wavevector, k_F, of the metal.[51] In general, the quantum efficiency of energy transfer can be written as

$$\Phi = \frac{1}{1+\left(\frac{r}{r_o}\right)^n} \quad (18)$$

such that in the case of dipole−dipole energy transfer, $n = 6$ and $r_o = R_o$, while for dipole−surface energy transfer, $n = 4$ and $r_o = d_o$, where r is the distance of the chromophore to the metal acceptor.[50]

Because of varying surface roughness for the different surface geometries in this report, the value of r will vary, but we assume that the quantitative measurements are representative of an ensemble average of PtOEP molecular environments throughout the 40 nm PVC film. Thus, r is considered to be constant, and the transfer rate is presumed to be equivalent for both 20 and 80 nm colloidal substrates. We attribute the different photophysical properties for PtOEP complexes in the PVC films on colloid-coated substrates to the sizes of the metal colloids themselves (a) and their respective surface area coverage.

Because the emission enhancements from fluorophores in the vicinity of metal colloids are proportional to colloid size, we expected that the emission intensity enhancement for the PtOEP/PVC samples on 80 nm Ag colloid/glass substrates should be larger than the enhancement for the chromophores in the presence of the 20 nm Ag colloids.[23−25,54] Conversely, we observed equivalent free space phosphorescence enhancements on the glass substrates coated with 20 nm colloids (Figure 2c, left) and 80 nm colloids (Figure 2d, left). We believe that we can ascribe this discrepancy to the differences in the concentrations of the 20 and 80 nm Ag colloid solutions. While the absorption for the glass and gold substrates modified with 20 and 80 nm colloids was not detectable (<0.001, data not shown), the concentration of the 20 nm particles is approximately 70 times greater than the concentration of the 80 nm particles. Thus, we expected that substrates incubated with 20 nm colloids had greater particle surface coverage, which resulted in a corresponding increase in the emission enhancement for the PtOEP/PVC samples on the 20 nm Ag colloid substrates.[55,56]

On the gold substrates (Figure 2b, left), the free space phosphorescence intensity is more enhanced than the free space emission from glass (Figure 2a, left). Because the evaporated gold metal layer acts as a mirror and reflects most of the otherwise transmitted light below the critical angle, θ_c, this is an expected result.[2] For the gold substrates, we also observe that the free space phosphorescence from the PtOEP/PVC samples on the 20 nm Ag colloid/gold substrate (Figure 2e, left) is greater than that from the 80 nm Ag colloid/gold substrates (Figure 2f, left). Again, we believe that this enhancement may in part be due to the greater surface coverage for the 20 nm colloids on the gold substrates.

From the surfaces coated with the silver colloids, we measured both long and short lifetime components (Table 1). The longer lifetime components for the free space phosphorescence emission for silver colloid-coated surfaces on the gold (20 nm, 55.6 μs; 80 nm, 55.5 μs) and glass substrates (20 nm, 56.6 μs; 80 nm, 62.0 μs) are slightly longer than the lifetimes on the uncoated glass (47.2 μs) and gold substrates (51.5 μs). We believe that the nature of these slightly longer components may be a result of less oxygen quenching due to the silver film roughness, which is on the order of 10 nm for the 20 nm particles and 40 nm for the 80 nm particles. With film thicknesses of approximately 10 and 40 nm, it is conceivable that the molecules on the rough surfaces can fill the crevices between adjacent silver colloids and be less exposed to the surrounding oxygen of the atmosphere.[32] Because we would expect deeper gaps for the substrates coated with the 80 nm colloids than those from the 20 nm colloids, the longer lifetime components for the glass substrates coated with 80 nm colloids (62.0 μs) versus those coated with 20 nm colloids (56.6 μs) are consistent with the hypothesis that the degree of oxygen quenching is related to the presence of crevices in rough colloidal surfaces.

With respect to the short lifetime components on the Ag colloid-coated substrates, we found that the lifetime components for PtOEP/PVC samples on the 80 nm silver colloid samples (glass, 4.82 μs; gold, 5.76 μs) were shorter than the lifetime components for PtOEP/PVC samples on the 20 nm samples (glass, 6.58 μs; gold, 7.78 μs). Although, exact values for the metal-modified radiative decay rate (Γ_m) have not yet been determined, these results are consistent with radiative plasmon model, which predicts that the lifetimes of chromophores in the presence of subwavelength silver colloids will decrease (radiative rates increase) with increasing radii of metal particles.[6,24,25] In addition, these short lifetime components are consistent with the values determined for PtOEP complexes on nanotextured silver surfaces.[32] This effect scales nicely with the scattering portion (eq 3) of the extinction as shown in Figure 3; hence, a greater intensity is expected for larger particles.[25]

Greater surface coverage from the 20 nm colloid samples on the glass substrates is further substantiated by the amplitude-weighted lifetime results (Table 1). The amplitude-weighted lifetime for the PtOEP/PVC samples on the substrates coated with the 20 nm colloids (40.2 μs) are shorter than the amplitude-weighted lifetimes of PtOEP/PVC samples on the substrates coated with the 80 nm colloids (52.9 μs). Because the short lifetime component for the PtOEP/PVC samples on the 80 nm Ag colloid samples (glass, 4.82 μs; gold, 5.76 μs) were shorter than the lifetime components for the 20 nm Ag colloid samples (glass, 6.58 μs; gold, 7.78 μs), the shorter amplitude-weighted lifetime for the PtOEP/PVC on 20 nm colloids substrates is reflective of a greater contribution of the shorter lifetime component for the metal-enhanced free space phosphorescence from the 20 nm Ag colloid-treated substrates. Thus, this provides further evidence to support the claim that the 20 nm colloids have a greater surface coverage on the glass and gold substrates.

As previously reported results for metal-enhanced fluorescence suggest, the decreased lifetimes or increased radiative decay rates for the fluorophore−metal particle systems imply that the fluorophores spend less time in the excited-state, thus increasing their photostability.[7,8,14,18,57] For the phosphorescent−metal particle system, the reported system lifetimes and photostability results reported are consistent with this model. As was described above, the lifetime components for chromophores in the presence of the 80 nm Ag colloids are shorter than those in the presence of the 20 nm Ag colloids. Hence, the RPM predicts that the PtOEP complexes will have a greater MEF component in the presence of the larger 80 nm colloids and a subsequent increase in photostability. Subsequently, we observe that the PtOEP complexes in the presence of substrates modified with 80 nm colloids are more photostable (glass, 2.12×10^{-2} sec^{-1}; gold, 1.69×10^{-2} sec^{-1}) than those modified with 20 nm colloids (glass, 2.88×10^{-2} sec^{-1}; gold, 2.01×10^{-2} sec^{-1}), which is consistent with the RPM.

5.2. ME-SPCP. With respect to plasmon-coupled emission on the continuous gold films with 47 nm thicknesses, system emission enhancement or quenching effects are due to the existence of three possible decay mechanisms for an excited-state population: (1) lossy surface waves (quenching), (2) transfer to surface plasmons (MEP), or (3) decays to far-field radiation (phosphorescence).[23] The extent of radiative transfer to surface plasmons has been shown to depend on the distance of separation between the chromophore and a continuous metal surface (r), the wavelength of the coupling radiation, and the dielectric properties of the metal surface (eq 6).[9,40,45,54,58] It has been suggested that the efficiency of energy transfer from an excited-state donor to a metal surface acceptor approaches unity for a chromophore in the presence of a metal surface in the near-field limit.[24]

With the observation of enhanced free space phosphorescence and the presence of a short lifetime component, we confirmed our observation of metal-enhanced phosphorescence for the PtOEP complexes in PVC films in the presence of Ag colloids on both glass and gold substrates. In addition to the free space intensity measurements for the colloids on the gold substrates, we also measured the photostabilities, lifetimes, and intensities of the SPCP signals for the different sample configurations on gold films. Consistent with the free space phosphorescence lifetime and photostability data trends, we observed the shortest lifetime and least photostability for the SPCP signal from the PtOEP/PVC samples on the 20 nm Ag colloid/gold substrates (44.5 μs). On the other hand, when the free space metal-enhanced phosphorescence lifetimes were compared to the SPCP lifetimes, we noticed that the lifetime for the PtOEP/PVC sample on the 20 nm Ag colloid/gold substrate (44.5 μs) was shorter than the lifetimes of the PtOEP/PVC samples on the gold substrates with no colloids (52.9 μs) and 80 nm Ag colloids (50.7 μs). This result not only contradicts the proposed plasmon model that suggest that the lifetimes of chromophores in the presence of subwavelength silver colloids (radiative rates increase) decrease with increasing radii of metal particles,[24,25,54] but it also contradicts the free space phosphorescence lifetime data trends for the colloid-treated glass substrates (Table 1). Although the greatest free space phosphorescence signal is from the PtOEP/PVC samples on the 20 nm Ag colloid/gold substrates, which is partly explained by the increased surface concentration of 20 nm silver colloids, we note only a minor enhancement of the SPCP signal from the Au films coated with 20 nm Ag colloids (Figure 2e, right). In addition, the SPCP signal from PtOEP/PVC sample on the gold substrates treated with the 20 nm silver colloids is the least photostable (3.32×10^{-2} sec^{-1}). The SPCP signal from the PtOEP/PVC samples on the gold films with no colloids had the longest lifetime, yet it was not the most photostable (1.04×10^{-2} sec^{-1}). Conversely, the PtOEP/PVC sample on the 80 nm Ag colloid/gold substrate had the most significant metal-enhanced plasmon-coupled phosphorescence signal (Figure 2f, right,) and is more photostable (5.00×10^{-3} sec^{-1}) than the SPCP signal from the gold substrate with no colloids (1.04×10^{-2} sec^{-1}) and 20 nm Ag colloids (3.32×10^{-2} sec^{-1}).

To explain these results, we draw on the quenching properties of metallic surfaces. As previously suggested, excited-state populations can decay by: (1) lossy surface waves, (2) transfer to surface plasmons, or (3) decays to far-field radiation.[23] Electrodynamic calculations have shown that above 300 nm distances decay processes occur through far-field radiation; from about 10−300 nm decay processes can transfer to surface plasmons, and typically below 10 nm excited-state populations decay through lossy surface waves (i.e., quenching).[23] As a result, we expect that the PtOEP/PVC samples on the 20 nm Ag colloid (10 nm radius, which is within the quenching limit) gold substrates will couple less effectively to the gold films due to the dominant quenching process. Consequently, the decreased SPCP signal, decreased SPCP photostability, and shorter SPCP lifetime for PtOEP/PVC samples on the 20 nm Ag colloid/gold substrates are suggestive of the presence of a substantial quenching component.

Since we have already shown an enhanced phosphorescence signal in the presence of the 20 nm silver colloids on glass substrates (Figure 2e, left), it follows that the SPCP phosphorescence is likely quenched substantially in the presence of 20

nm silver colloids on gold films (Figure 2e, right) than in their absence. In summary, the chromophore couples to the 20 nm Ag colloid, and the colloid couples to the plasmons in the gold film, but because the colloid size is within the quenching limit for the gold film, we observe little SPCP signal, decreased photostability, decreased lifetime, and increased quenching. Furthermore, the greater the degree of coupling of the phosphorescence to the 20 nm silver colloids, the more closely we would expect the photostabilities, lifetimes, and intensities of the SPCP signal for the gold/20 nm colloid geometry to compare to the respective results from PtOEP samples on plain gold films. This result is confirmed by the reported photostability and intensity results, giving us confidence in our interpretations.

Interestingly, the SPCP from the PtOEP/PVC sample on the 80 nm Ag colloid/gold substrates was the most photostable (Figure 4, right). These results suggest that as a result of the metal-enhanced phosphorescence coupling to the surface plasmons in the gold film, the system radiative decay rate for the chromophore increases. As a result, the excited-state energy of the fluorophores−metal system transfer more effectively to surface plasmons and quenching is minimized. In addition, the metal-enhanced free space phosphorescence amplitude-weighted lifetime from the PtOEP/PVC sample on the glass substrates with 80 nm silver colloids were longer than the phosphorescence lifetimes for the PtOEP/PVC samples on the gold substrates with silver colloids (Table 1), which further suggests that the increased photostability on the gold substrates coated with the 80 nm Ag colloids is related to the metal-enhanced plasmon-coupling phenomenon. Because of the larger-sized 80 nm silver colloids, we expect that the quenching phenomenon is minimized and plasmon-coupled emission becomes the dominant phenomenon. The significant ME-SPCP signal observed (Figure 2f, right) demonstrates the significant phosphorescence enhancements achieved by combining the benefits of MEP with SPCP.

6. Conclusions

In conclusion, we have successfully demonstrated the phenomenon of ME-SPCP. We have confirmed the presence of MEP for the Ag colloid-treated gold and glass substrates with the lifetime, photostability, and intensity measurements for the free space phosphorescence of PtOEP/PVC samples. We attribute the longer component lifetime to free space phosphorescence emission, and the shorter lifetime component signifies the presence of metal-enhanced phosphorescence. Free space phosphorescence intensity enhancements and lifetime measurements for the PtOEP complexes in PVC films on the colloid-treated substrates provide further evidence for the existence of the radiating plasmon model.[24,25]

In addition to the confirmation of MEP from the PtOEP/PVC samples in the presence of Ag colloids on gold substrates, we also demonstrated significant enhancements of SPCP signal in the presence larger 80 nm Ag colloids. From these results, we notice a pronounced enhancement of the SPCP signal, increased photostability, and slightly shortened SPCP lifetime from the PtOEP/PVC samples on the 80 nm Ag colloid/gold substrates. We also note a minor enhancement of the SPCP signal from the PtOEP/PVC samples on the 20 nm Ag colloid/gold substrates, but provide evidence for the quenching of ME-SPCP in the presence of the smaller Ag colloid/gold substrates.

The SPCP enhancement from the PtOEP/PVC samples gold films-coated Ag colloids is the first observation of ME-SPCP. In addition, we believe that this is the first observation of two populations of plasmons: ME-SPCP and MEP. With the dramatic signal enhancements and improved photostability associated with ME-SPCP, we believe that ME-SPCP can be incorporated into new high-sensitivity, robust-sensing technologies, such as the detection of biomolecular interactions on/at surfaces from weakly emitting phosphorescing species(i.e., protein dynamics and alkaline phosphatase studies) or to detect highly dilute solutions of biomolecules (i.e., bioterroism agents).

Acknowledgment. This work was supported by the NIH, National Center for Research Resources, RR008119. Support to the authors from UMBI, CFS, and IOF is also acknowledged.

References and Notes

(1) Liedberg, B.; Nylander, C.; Lundstrom, I. *Biosens. Bioelectron.* **1995**, *10*, R1.
(2) Liebermann, T.; Knoll, W. *Colloids Surf., A* **2000**, *171*, 115.
(3) Liebermann, T.; Knoll, W.; Sluka, P.; Herrmann, R. *Colloids Surf., A* **2000**, *169*, 337.
(4) Lakowicz, J. R. *Anal. Biochem.* **2001**, *298*, 1.
(5) Kambhampati, D.; Nielsen, P. E.; Knoll, W. *Biosens. Bioelectron.* **2001**, *16*, 1109.
(6) Aslan, K.; Gryczynski, I.; Malicka, J.; Matveeva, E.; Lakowicz, J. R.; Geddes, C. D. *Curr. Opin. Biotechnol.* **2005**, *16*, 55.
(7) Drexhage, K. H. *Ber. Bunsen-Ges.* **1968**, *72*, 329.
(8) Chance, R. R.; Prock, A.; Silbey, R. *J. Chem. Phys.* **1974**, *60*, 2744.
(9) Morawitz, H.; Philpott, M. R. *Phys. Rev. B* **1974**, *10*, 4863.
(10) Glass, A. M.; Liao, P. F.; Bergman, J. G.; Olson, D. H. *Opt. Lett.* **1980**, *5*, 368.
(11) Gersten, J.; Nitzan, A. *J. Chem. Phys.* **1981**, *75*, 1139.
(12) Sokolov, K.; Chumanov, G.; Cotton, T. M. *Anal. Chem.* **1998**, *70*, 3898.
(13) Johansson, P.; Xu, H. X.; Kall, M. *Phys. Rev. B* **2005**, *72*.
(14) Tews, K. H. *Ann. Phys.* **1973**, *29*, 97.
(15) Kreschmann, E.; Raether, H. *Z. Naturforsch., A.* **1968**, *23*, 2135.
(16) Philpott, M. R. *Chem. Phys. Lett.* **1973**, *19*, 435.
(17) Weitz, D. A.; Garoff, S.; Hanson, C. D.; Gramila, T. J.; Gersten, J. I. *Opt. Lett.* **1982**, *7*, 89.
(18) Weitz, D. A.; Garoff, S.; Hanson, C. D.; Gramila, T. J.; Gersten, J. I. *J. Lumin.* **1981**, *24*−*5*, 83.
(19) Ritchie, G.; Burstein, E. *Phys. Rev. B* **1981**, *24*, 4843.
(20) Weitz, D. A.; Garoff, S.; Gersten, J. I.; Nitzan, A. *J. Chem. Phys.* **1983**, *78*, 5324.
(21) Wokaun, A. *Mol. Phys.* **1985**, *56*, 1.
(22) Wokaun, A.; Lutz, H. P.; King, A. P.; Wild, U. P.; Ernst, R. R. *J. Chem. Phys.* **1983**, *79*, 509.
(23) Ford, G. W.; Weber, W. H. *Phys. Rep.* **1984**, *113*, 195.
(24) Lakowicz, J. R. *Anal. Biochem.* **2005**, *337*, 171.
(25) Aslan, K.; Leonenko, Z.; Lakowicz, J. R.; Geddes, C. D. *J. Fluoresc.* **2005**, *15*, 643.
(26) Lukomska, J.; Malicka, J.; Gryczynski, I.; Leonenko, Z.; Lakowicz, J. R. *Biopolymers* **2005**, *77*, 31.
(27) Lukomska, J.; Malicka, J.; Gryczynski, I.; Lakowicz, J. R. *J. Fluoresc.* **2004**, *14*, 417.
(28) *Radiative Decay Engineering*; Geddes, C. D.; Lakowicz, J. R., Eds.; Springer: New York, 2005; Vol. 8.
(29) Kang, J. S.; Piszczek, G.; Lakowicz, J. R. *J. Fluoresc.* **2002**, *12*, 97.
(30) Geddes, C. D.; Lakowicz, J. R. *J. Fluoresc.* **2002**, *12*, 121.
(31) Maliwal, B. P.; Gryczynski, Z.; Lakowicz, J. R. *Anal. Chem.* **2001**, *73*, 4277.
(32) Pan, S. L.; Rothberg, L. J. *J. Am. Chem. Soc.* **2005**, *127*, 6087.
(33) Zhang, Y.; Aslan, K.; Malyn, S. N.; Geddes, C. D. *Chem. Phys. Lett.* **2006**, *427*, 432.
(34) Benner, R. E.; Dornhaus, R.; Chang, R. K. *Opt. Commun.* **1979**, *30*, 145.
(35) Weber, W. H.; Eagen, C. F. *Bull. Am. Phys. Soc.* **1979**, *24*, 441.
(36) Weber, W. H.; Eagen, C. F. *Opt. Lett.* **1979**, *4*, 236.
(37) Knobloch, H.; Brunner, H.; Leitner, A.; Aussenegg, F.; Knoll, W. *J. Chem. Phys.* **1993**, *98*, 10093.
(38) Gryczynski, I.; Malicka, J.; Gryczynski, Z.; Lakowicz, J. R. *Anal. Biochem.* **2004**, *324*, 170.
(39) Lakowicz, J. R. *Anal. Biochem.* **2004**, *324*, 153.
(40) Philpott, M. R. *J. Chem. Phys.* **1975**, *62*, 1812.
(41) Previte, M. J. R.; Aslan, K.; Zhang, Y.; Geddes, C. D. *Chem. Phys. Lett.*, in press.
(42) Liedberg, B.; Lundstrom, I.; Stenberg, E. *Sens. Actuators, B* **1993**, *11*, 63.
(43) Melendez, J.; Carr, R.; Bartholomew, D. U.; Kukanskis, K.; Elkind, J.; Yee, S.; Furlong, C.; Woodbury, R. *Sens. Actuators, B* **1996**, *35*, 212.

(44) Salamon, Z.; Macleod, H. A.; Tollin, G. *Biochim. Biophys. Acta* **1997**, *1331*, 131.
(45) Burstein, E.; Chen, W. P.; Chen, Y. J.; Hartstein, A. *J. Vac. Sci. Technol.* **1974**, *11*, 1004.
(46) Hansen, W. N. *J. Opt. Soc. Am.* **1968**, *58*, 380.
(47) Gryczynski, I.; Malicka, J.; Nowaczyk, K.; Gryczynski, Z.; Lakowicz, J. R. *J. Phys. Chem. B* **2004**, *108*, 12073.
(48) Yguerabide, J.; Yguerabide, E. E. *Anal. Biochem.* **1998**, *262*, 137.
(49) Yguerabide, J.; Yguerabide, E. E. *Anal. Biochem.* **1998**, *262*, 157.
(50) Yun, C. S.; Javier, A.; Jennings, T.; Fisher, M.; Hira, S.; Peterson, S.; Hopkins, B.; Reich, N. O.; Strouse, G. F. *J. Am. Chem. Soc.* **2005**, *127*, 3115.
(51) Chance, R. R.; Prock, A.; Silbey, R. *Adv. Chem. Phys.* **1978**, *37*, 1.
(52) Persson, B. N. J.; Lang, N. D. *Phys. Rev. B* **1982**, *26*, 5409.
(53) Dulkeith, E.; Morteani, A. C.; Niedereichholz, T.; Klar, T. A.; Feldmann, J.; Levi, S. A.; van Veggel, F.; Reinhoudt, D. N.; Moller, M.; Gittins, D. I. *Phys. Rev. Lett.* **2002**, *89*.
(54) Messinger, B. J.; Vonraben, K. U.; Chang, R. K.; Barber, P. W. *Phys. Rev. B* **1981**, *24*, 649.
(55) Grabar, K. C.; Freeman, R. G.; Hommer, M. B.; Natan, M. J. *Anal. Chem.* **1995**, *67*, 735.
(56) Geddes, C. D.; Cao, H.; Gryczynski, I.; Gryczynski, Z.; Fang, J. Y.; Lakowicz, J. R. *J. Phys. Chem. A* **2003**, *107*, 3443.
(57) Weitz, D. A.; Garoff, S.; Hanson, C. D. *Bull. Am. Phys. Soc.* **1981**, *26*, 339.
(58) Kretschmann, E. *Z. Phys.* **1971**, *241*, 313.
(59) [a]All photostability data was fit with a double exponential decay: $I(t) = A_1e^{-k_1t} + A_2e^{-k_2t}$.